Helium retention with dislocations in deformed pure iron

Y.H. Gong[a], X.Z. Cao[a,*], S.X. Jin[a], E.Y. Lu[a], Y.C. Hu[a], T. Zhu[a], P. Kuang[a], Q. Xu[b], B.Y. Wang[a]

[a]*Institute of High Energy Physics, Chinese Academy of Sciences, Beijing 100049, China*

[b]*Research Reactor Institute, Kyoto University, Osaka 590-0494, Japan*

Abstract

Effects of deformed dislocation on helium retention in pure iron, including the helium atoms diffusion along the dislocation line and desorption from dislocation trapping sites, were investigated. The dislocation defect was introduced in specimens by cold-rolling, and then 5 keV helium ions were implanted into the deformed specimens. Slow positron beam technology and thermal desorption spectroscopy were used to investigate the evolution of dislocation defects and the desorption behavior of helium atoms under influence of dislocation. The behaviors of S-E, W-E and S-W plots indicate clearly that lots of helium atoms remain in the deformed specimen and helium atoms combining with dislocation change the distribution of electron density. The helium desorption plot indicates that dislocation accelerates helium desorption at 293 K-600 K and facilitates helium dissociation from He_nV_m (n/m=1.8) cluster.

Keywords: Helium diffusion; Dislocation; Thermal desorption; Positron annihilation

1. Introduction

Irradiation hardening, swelling and helium embrittlement are the main problems in first-wall materials of nuclear fusion reactor. These problems have relations with helium atoms in the material, and helium atoms were generated almost due to the (n, α) nuclear reaction [1, 2]. It is well known that the helium atoms have low migration energy and low solubility in iron-based alloy, and have strong interaction with the micro-defects, such as vacancies, dislocations, grain boundaries and vacancy clusters. As a result, the helium atoms were easily trapped by the micro-defects and aggregated to form He_nV_m clusters nearby the micro-defects, which increase the ductile brittle transition temperature of materials. Eventually, helium embrittlement is considered as one of the menaces to the reactor safety. Many researchers have been committed to focus on helium embrittlement, helium bubbles formation and materials swelling phenomenon [3-6], and also paid attention to effects of micro-defect on helium atoms migration. Noteworthy, helium atoms, as the impurity atoms, can easily diffuse along the dislocation line direction [7-9]. Xu et al. reported that the dislocation-trapped helium could affect the mechanical properties of pure iron, and the deformation dislocations can enhance the helium diffusion along dislocation line [10]. The interaction between dislocations and helium atoms has attracting researchers, which is benefit for understanding helium aggregation, nucleation and growth mechanism nearby the dislocation.

The reduced activation ferritic/martensitic steels are one of the candidate structural materials for fusion reactor. The nuclear structural materials including Eurofer 97,

* Corresponding Author. E-mail address: caoxzh@ihep.ac.cn. TEL: +86-10-8823-5971

CLAM, F82H and Fe9Cr2WVTa, are iron based alloy. In order to investigate the interaction between dislocation and helium, pure iron which has similar lattice structure to aforesaid nuclear structural materials was used in present study.

Positron annihilation Doppler broadening spectroscopy (DBS) is usually used to characterize micro-defect evolution because the positrons were easily trapped in micro-defects and annihilated with electron around micro-defects. The results of DBS can be used to analyze the change information of defects [11]. Thermal desorption spectrum (TDS) is an effective experimental methods to observe the helium desorption behavior in materials. Helium desorption activation energy with the temporal temperature can be estimated from the relationship between the helium desorption rate and heating time. In this paper, the interaction between dislocation and helium atoms was analyzed by DBS and TDS.

2. Experimental procedure

Polycrystalline iron was used and the iron (purity: 99.99%) was cut to 10 ×10 mm with a thickness of 0.3 mm. All specimens were annealed at 1023 K for 2 h in vacuum (~10^{-5} Pa). In order to introduce dislocation defects, the well-annealed specimens were rolled 10% thickness reduction by cold rolling machine. And then, the specimens were annealed at 673 K for 1 h in vacuum (~10^{-5} Pa) to eliminate the vacancy type defects [12], and reserve the dislocation type defects in the matrix, the transmission electron microscope (TEM) images of the well-annealed specimen, before and after 673 K annealed of deformed specimen were shown in Fig. 1. Before the helium implantation, all specimens were chemically polished to clean the surface. Helium implantation was carried out using 5 keV He^+ with a flux of 5.0×10^{17} He^+/m^2s at room temperature, and the total irradiation dose was 1×10^{20} He^+/m^2.

DBS of slow positron beam was carried out to characterize the defect depth distribution. Positrons are generated by 45 mCi ^{22}Na (2014) radiation source and moderated by solid Ne moderator. The single HPGe detector was used in DBS measurement to detect the emitted γ rays by positron annihilation. The monoenergetic positrons were implanted into the specimens with the energy varied from 0.1 keV to 20 keV. S and W parameters were usually used to describe the momentum distribution of annihilated electron. S parameter is defined as the ratios of the central area counts for low Doppler-shift (510.2 keV-511.8 keV) and W parameter is defined as the two flanks regions counts for high Doppler-shift (504.2 keV-508.4 keV and 513.6 keV-517.8 keV) in the DB spectra to the total counts. The total counts of the DB spectrum is accumulated to 2.0×10^6 to reduce the statistical error.

TDS was widely used for studying helium desorption processes as a usual experimental tool [13, 14]. In this experiment, the temperature is ramping with 1 K/s from 293 K to 1400 K by infrared radiation heater. During heating, helium was monitored by a quadrupole mass analyzer in a vacuum of 10^{-6} Pa.

3. Results

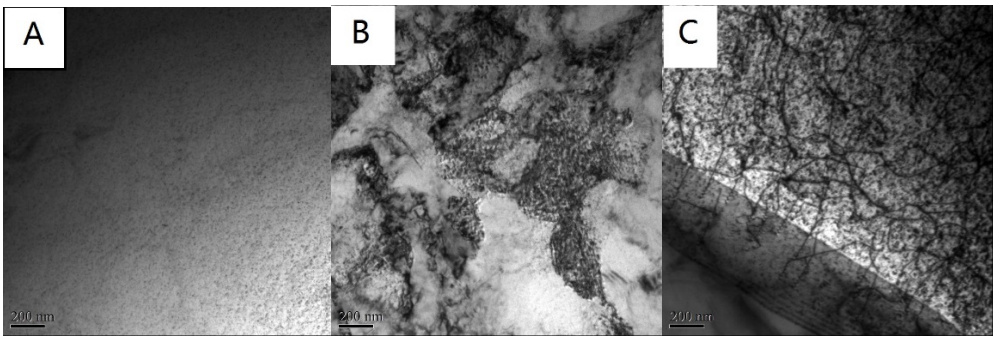

Fig. 1. TEM result for microstructure of dislocation. (a): well-annealed specimen, (b): deformed specimen, (c): deformed specimen and annealed at 673 K for 1 h.

The microstructure of dislocations were shown in Fig. 1. The well-annealed specimen has little dislocation and the deformed specimen has lots of dislocation in the dark area. After 673 K annealed for deformed specimen, there are still lots of dislocation. In the positron annihilation lifetime test, the positron lifetime of well-annealed specimen was 105.9 ps. The long lifetime τ_2 was changed from 150 ps (deformed) to 117.3 ps (673 K annealed). It demonstrates that deformed specimen annealed at 673 K which can eliminate the vacancy type defects and reserve the dislocation type defects in the matrix.

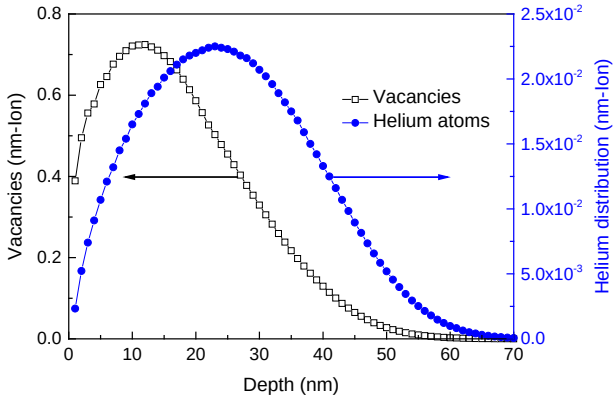

Fig. 2. Profiles of vacancies and helium atoms distribution in iron implanted with 5 keV He^+ calculated with SRIM2013.

The distribution of implanted helium and produced vacancies were simulated by SRIM, as shown in Fig. 2. The displacement energy of Fe was set to 40 eV [15]. SRIM calculation demonstrates that the approximate helium maximum penetration depth is only 84 nm. The vacancy peak and helium distribution peak locates at ~12 nm and ~23 nm, respectively.

S and W parameters as a function of incident positron energy are shown in Fig. 3, and the positron implantation depth is estimated using the following experimental equation [16]. The calculated results are also shown on the upper horizontal scale in Fig. 3.

$$Z(E) = \frac{40000E^{1.6}}{\rho}, \quad (1)$$

where Z is expressed in units of nm, ρ is the density in units of kg/m^3, the density of

pure iron is 7.86×10^{3}kg/m^{3} in present experiment, and E is the positron energy in units of keV.

It is shown that the S parameters of all specimens were larger at low incident positron energies (the range of 0.1 keV ~ 2.0 keV), which was due to the surface effect, including the production of ortho-positronium and the positrons backscattering [17]. Subsequently, the S parameter decreased with the positron energy increasing and then tend to be stable when the energy is above 11 keV. The area was named stable area where from 11 keV to 20 keV. For the deformed specimen, the S parameter was larger than that of well-annealed specimen in the stable area. After helium implantation, the S parameter of deformed specimen decreased. The W parameter of well-annealed specimen is larger than that of deformed specimen in the stable area before helium implantation. After helium implantation, the W parameter of well-annealed specimen is still larger than that of deformed specimen, but the increment is smaller than that of deformed specimen.

Moreover, the S-W plot was used to describe the positron annihilation mechanism with different type of defect [18]. The dots showing a linear relationship means that the positron annihilation mechanism did not change, which indicates that there may be only one type of defect in the specimen. The S-W curves slope was associated with the type of defect. The S-W curves of well-annealed and deformed specimens were shown in Fig. 4. Before helium implantation, the S-W curve of well-annealed specimen demonstrate a linear relationship, whereas the dots of deformed specimen were concentrated in the stable area. After helium implantation, the S-W curves of both well annealed and deformed specimen were similar with the result of unirradiated annealing one, and they demonstrate a linear relationship.

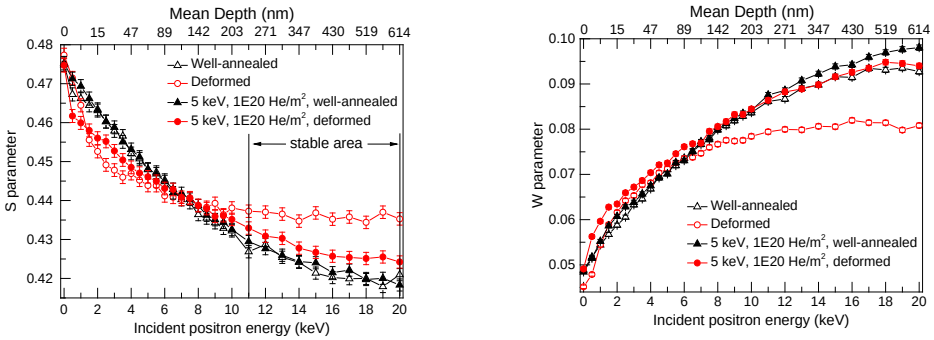

Fig. 3. S and W parameter as a function of incident positron energy (mean implantation depth) in unirradiated and irradiated iron

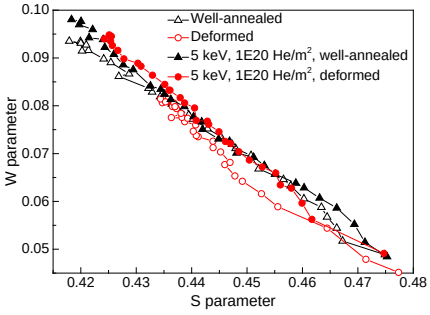

Fig. 4. W-parameter as a function of the S-parameter for well-annealed and deformed iron

Fig. 5 shows the TDS results of well-annealed specimen and deformed specimen, respectively. The specimens were irradiated by 5 keV He^+ ions with a dose of 1.0×10^{20} He^+/m^2 at room temperature. The helium desorption peaks of well annealed specimen in Fig. 5(A) were at 683 K (peak a), 780 K (peak b), 1180 K (peak c), 1209 K (peak d), 1270 K (peak e) and in the range from 800 K to 1100 K, respectively. Fig. 5(B) is the result of deformed specimen, and the helium desorption peaks were at 550 K (peak 1), 800 K (peak 2), 1047 K (peak 3), 1135 K (peak 4), 1270 K (peak 5) and in the range from 800 K to 1100 K, respectively.

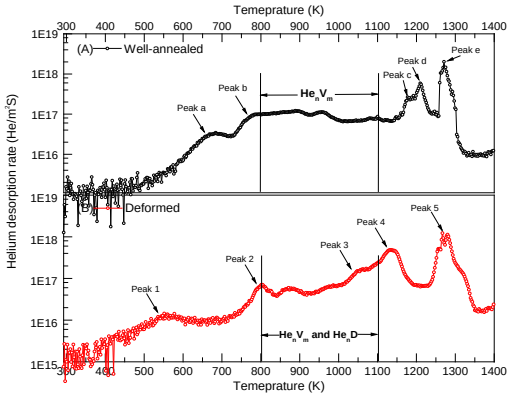

Fig. 5. Helium thermal desorption spectra for iron. (A): 5 keV He^+ ions irradiated in well-annealed iron and (B): 5 keV He^+ ions irradiated in deformed iron.

4. Discussion

The S parameter describes the information of positron annihilated with valence electron and reflects the information of the micro-defects. The numerical value of S parameter is related to the type, density and size of defects. There are lots of dislocations in the deformed specimen before helium implantation. In previous study, the dislocation density of 10% deformed specimen was estimated to be $10^9/cm^2$ [19, 20]. Therefore, positrons were easily trapped by dislocations and have higher probability annihilated with valence electron. Ignoring the surface effect, the S parameter of deformed specimen is higher than that of well-annealed specimen in the stable area. After helium implantation, many vacancies and helium atoms are introduced in the damage area distributes around at 12 nm according to the SRIM calculation. It is well known that helium atoms can diffuse easily in iron due to the low migration energy (0.078 eV) [21]. In addition, the migration energy of vacancy is 0.78 eV in defect-free iron [22]. Therefore, vacancy migration is more difficult than helium migration in the matrix at the room temperature. Xu et al. reported that the 100 eV He^+ with a flux of 5.0×10^{15} He^+/m^2s implanted in deformed pure iron specimen and the total dose was 1.0×10^{20} He^+/m^2, the helium atoms concentration could reach 1.2 ppm in 1000 nm of the surface in the deformed specimen [10]. In addition, helium has negative affinity for electrons, which lead the probability of positron annihilation with the valence electron decreased [23]. Therefore, The S parameter of the deformed specimen decreased in the stable area. For well-annealed specimen, the S parameter is almost no change because

of there are few vacancy type defects in the stable area. Therefore, whether helium atoms exist or not in the stable area, the S parameter of well-annealed specimen is almost no change. The W parameter will be affected if the helium atoms exist in the stable area. W parameter reflected the information of positron annihilation with the high momentum electron. After helium implantation, helium trapped by dislocation which lead the effective positron trapping state density decreased and the probability of positron annihilation with high momentum electron was increased in the stable area. The increment of W parameter has negative correlation with effective positron trapping state density. Obviously, it indicates that there are more helium atoms remain in deformed specimen than that in well-annealed specimen in the stable area.

Before helium implantation, the S-W curve of the well-annealed specimen is fitted as a linear function. However, the range of the S-W curve in the deformed specimen is shorter than that for the well-annealed specimen, which is due to the formation of dislocation defects. After helium implantation, a new type defect (i.e., helium cluster - dislocation He_nD) formed due to the combination of helium atoms and dislocations, which changed the probability of positron annihilation with the electron around dislocations. So that the S-W curve of the deformed specimen is fitted as a linear function after helium implantation.

The thermal desorption spectroscopy indicates that the helium desorption peaks with a constant heating rate correspond to the release of helium atoms from different trapping sites. Based on simple first order dissociation kinetics, the helium desorption activation energy was calculated with the followed equation, i.e. [24]:

$$\frac{dN}{dt} = -fN\exp\left(\frac{-E}{K_B T}\right), \quad (2)$$

Where N is the number of helium atoms remaining and not yet desorbed from a trapping state, f is the jumping frequency (assumed to be 10^{13}/s), E is the helium desorption activation energy for the trap, and K_B is the Boltzmann constant. Desorption peak temperature Tp, heating rate β and helium desorption activation energy E have the derived relationship, i.e. [24, 25]:

$$\ln\left(\frac{\beta}{T_p^2}\right) = -\frac{E}{(K_B T_p)} + \ln\left(\frac{fK_B}{E}\right). \quad (3)$$

In this TDS experiments, the heating rate β was fixed at 1 K/s, the helium desorption energy E was reckon as [26],

$$E = 0.0029T_p. \quad (4)$$

The desorption energy of helium atoms from defect were estimated by the above equation. The results of desorption energy are tabulated in Table 1.

Table 1

Desorption temperature and desorption energy

Desorption Temperature (K)	Peak and desorption energy (eV)

Fig. 5(A)	Fig. 5(B)	Fig. 5(A)	Fig. 5(B)
683	550	Peak a: 1.98	Peak 1: 1.60
780	800	Peak b: 2.26	Peak 2: 2.32
1180	1047	Peak c: 3.42	Peak 3: 3.04
1209	1135	Peak d: 3.51	Peak 4: 3.29
1270	1270	Peak e: 3.68	Peak 5: 3.68

After helium implantation, many vacancies were introduced in the specimen, and helium-vacancy (He_nV_m) clusters were formed due to the combination between vacancies and helium atoms, where n and m are the numbers of helium atoms and vacancies in clusters, respectively. The helium atoms stable configuration in the He_nV_m clusters primarily depends on the helium-to-vacancy ratio (n/m) of the cluster [26]. The binding energy of helium atoms to a He_nV_m cluster gradually decreased as helium-to-vacancy ratio increased.

Vacancy type defects introduced by helium ion irradiation start to recover at 673 K and completely recover near 1273 K [27]. With temperature increasing, the helium-to-vacancy ratio rises with the recovery of vacancy type defects. Therefore, helium atoms were easily dissociated from He_nV_m clusters when the helium-to-vacancy ratio increased. For the helium desorption curve in Fig. 5(A), peak a located at 683 K, which was considered as the vacancy recovery. But the peak 1 in Fig. 5(B) (550 K) appears before peak a. This is because many vacancies and helium atoms were trapped by dislocation which prevent the larger He_nV_m cluster formation. Vacancies could be detrapped from dislocation at 573 K [22], which lead to the helium-to-vacancy ratio increased near the dislocation area. Therefore, the peak 1 appear earlier than peak a. It indicates that dislocations promote helium atoms desorption from He_nV_m cluster at low temperature. Meanwhile, the helium atoms desorption rate of deformed specimen is larger than that of well-annealed specimen in the range from 293 K to 600 K, which demonstrate the helium atoms were easily dissociated due to dislocation existence at low temperature.

Table 2
Theoretical de-trapping energy and calculative desorption energy of helium in iron

$E_{migration}$ (eV)	$E_{binding}$ (eV)	$E_{de\text{-}trapping}$ (eV)	$E_{desorption}$ (eV)	Defect type
Bulk: 0.078	2.26	2.338	Peak b: 2.26 Peak 2: 2.32	dislocation
	2.87	2.948	Peak 3: 3.04	jog
	3.24	3.318	Peak c: 3.42 Peak 4: 3.29	vacancy

The theoretical de-trapping energy and calculative desorption energy of helium to different type defects are tabulated in Table 2. Helium irradiation also can introduce a few of dislocation type defects, and the dislocation begin to recover at about 800 K [22]. The de-trapping energy of helium atom from dislocation is 2.338 eV, which is the sum of the binding energy of helium atom to the dislocation (2.26 eV) and the migration

energy of helium atom to iron (0.078 eV). The desorption energy of helium atoms of peak b and peak 2 are 2.26 eV and 2.32 eV. Thus, peak b and peak 2 were assigned to the helium atoms desorption from dislocations. The range from 800 K to 1100 K of both Fig. 5(A) and Fig. 5(B) were assigned the helium atoms dissociated from He_nV_m clusters and dislocation networks (He_nD). Meanwhile, the size of He_nV_m cluster become larger and the helium-to-vacancy ratio shows a decrease first and then an increase with the temperature rising. For the deformed specimen, dislocations were interlaced and formed a segments of dislocation line. The segments of dislocation line which not belong to the original glide plane are jogs. The binding energy of the helium atoms to jog is 2.87 eV which is larger than helium atoms to dislocation (2.26 eV) [28]. It indicated that helium atoms combine with jogs were more stable than dislocations. The de-trapping energy of peak 3 in Fig. 5(B) is 3.04 eV, approximating the binding energy of the helium atoms to jogs (2.948 eV). Thus, peak 3 was regarded as helium atoms dissociation from jogs.

When the temperature above 1100 K, the helium-to-vacancy ratio was approximately equal to 1.8 and the He_nV_m cluster (n/m=1.8) begin to form the more stable and larger size helium bubble. The de-trapping energy of helium atom from He_nV_m cluster (n/m=1.8) is about 3.24 eV [27]. The desorption energy of helium atom of peak c and peak 4 was closed to 3.318 eV (=3.24 eV+0.078 eV). Peak c and peak 4 were assumed to be the helium atoms dissociation from He_nV_m cluster (n/m=1.8). However, peak 4 appears earlier than peak c. The possible reason is that vacancy self-diffusion mobility in deformed specimen was higher than that in well-annealed specimen [22]. The migration energy of vacancy along the dislocation was 1.25 eV, and the formation energy of vacancy in the dislocation core was 0.86 eV. The migration and formation energy of vacancy in bulk were 0.78 eV and 1.70 eV, respectively. Therefore, the self-diffusion energy of vacancy along the dislocation and in the bulk were 2.11 eV and 2.48 eV. The He_nV_m cluster migration, aggregation and growing process are dynamic process with the temperature rising, and the vacancy continually absorbed and released in the dynamic process. The dislocation may play a positive role in vacancy releasing, which lead the helium-to-vacancy ratio increased. So helium atoms were emitted from He_nV_m cluster (n/m=1.8) in order to keep the He_nV_m cluster (n/m=1.8) structure stable. Thus, the peak 4 appeared earlier than peak c. It can be infer that dislocation promote the helium desorption form He_nV_m cluster (n/m=1.8).

The temperature (~1185 K) was the lattice structure transformation point from BCC to FCC in pure iron. At this temperature, the defects were almost annihilated and amounts of helium atoms were released, so the helium desorption peak was sharpened. The sharpened peak d were observed in well-annealed specimen. However, there are no sharpened peak in deformed specimen, the most likely reason is that the migration and aggregation of He_nV_m clusters (n/m=1.8) will restrain by the existence of dislocation with the temperature rising. There will be more smaller-sized He_nV_m clusters in deformed specimen compared with well-annealed specimen. When the lattice structure beginning to change, there may exist a process that the smaller-sized He_nV_m clusters coalesce and form a larger helium bubbles rather than emit helium atoms. It indicates that the dislocation could restrain the larger-sized helium bubble formation. At last, the

peak e and peak 5 were assigned the dissociation from helium bubbles.

5. Conclusion

The effect of dislocation on helium diffusion and desorption in helium irradiated pure iron was studied by DBS and TDS. Helium atoms combined with dislocation change the type of defect (i.e., He_nD). Dislocation promotes the helium desorption at 293 K-600 K and promotes helium dissociation from He_nV_m clusters (n/m=1.8). The desorption energy of helium atoms from dislocation was estimated 2.32 eV in the deformed specimen and helium combined with jogs was more stable than dislocations. The existed dislocations in pure iron could restrain the formation of large-sized helium bubble.

Acknowledgements

This work is supported by the National Natural Science Foundation of China (11475193, 11575205 and 11505192).

References

[1] E.E. Bloom, The challenge of developing structural materials for fusion power systems, J. Nucl. Mater. 258 (1998) 7-17

[2] N. Yoshida, and Y. Hirooka, Impacts of charge-exchange neutrals on degradation of plasma-facing materials, J. Nucl. Mater. 258 (1998) 173-182

[3] J. Chen，Z.Y. He, and P. Jung, Microstructure of helium-implanted alpha-Al2O3 after annealing, Acta Mater. 54 (2006) 1607-1614

[4] R. Vassen，H. Trinkaus, and P. Jung, Helium desorption from Fe and V by atomic diffusion and bubble migration, Phys. Rev. B. 44 (1991) 4206-4213

[5] I. Chernov，A.N. Kalashnikov，B.A. Kahn, and S.Y. Binyukova, Gas bubbles evolution peculiarities in ferritic-martensitic and austenitic steels and alloys under helium-ion irradiation, J. Nucl. Mater. 323 (2003) 341-345

[6] D. Kramer，H.R. Brager，C.G. Rhodes, and A.G. Pard, HELIUM EMBRITTLEMENT IN TYPE 304 STAINLESS STEEL, J. Nucl. Mater. 25 (1968) 121-131

[7] G.R. Love, DISLOCATION PIPE DIFFUSION, Acta Metall Mater. 12 (1964) 731-737

[8] R.W. Balluffi, MEASUREMENTS OF SELF-DIFFUSION RATES ALONG DISLOCATIONS IN FCC METALS, Physica Status Solidi. 42 (1970) 11-34

[9] M.J. Turunen, and V.K. Lindroos, MODEL FOR DISLOCATION CLIMB BY A PIPE DIFFUSION MECHANISM, Philos. Maga. 29 (1974) 701-708

[10] Q. Xu，Y. Sugiura，X.Q. Pan，K. Sato, and T. Yoshiie, Effects of dislocation-trapped helium on mechanical properties of Fe, Mat. Sci. Eng:A. 612 (2014) 41-45

[11] Y.C. Wu，Y.Q. Chen，B. Wang，S.J. Wang，Y.C. Jean，R. Suzuki, and T. Ohdaira, Slow positron beam study of corrosion-related defects in pure iron, APPL. SURF. SCI. 252 (2006) 3274-3277

[12] X.Z. Cao，Q. Xu，K. Sato, and T. Yoshiie, Effects of dislocations on thermal

helium desorption from nickel and iron, J. Nucl. Mater. 417 (2011) 1034-1037
[13] D.A. King, THERMAL DESORPTION FROM METAL-SURFACES, Surf. Sci. 47 (1975) 384-402
[14] S.J. Lombardo, and A.T. Bell, A MONTE-CARLO MODEL FOR THE SIMULATION OF TEMPERATURE-PROGRAMMED DESORPTION SPECTRA, Surf. Sci. 206 (1988) 101-123
[15] C.D. Hardie，C.A. Williams，S. Xu, and S.G. Roberts, Effects of irradiation temperature and dose rate on the mechanical properties of self-ion implanted Fe and Fe-Cr alloys, J. Nucl. Mater. 439 (2013) 33-40
[16] J. Qiu，Y. Xin，X. Ju，L.P. Guo，B.Y. Wang，Y.R. Zhong，Q.Y. Huang, and Y.C. Wu, Investigation by slow positron beam of defects in CLAM steel induced by helium and hydrogen implantation, Nucl. Instrum. Methods Phys. Res., Sect. B. 267 (2009) 3162-3165
[17] E.Y. Lu，X.Z. Cao，S.X. Jin，P. Zhang，C.X. Zhang，J. Yang，Y.R. Wu，L.P. Guo, and B.Y. Wang, Investigation of vacancy-type defects in helium irradiated FeCrNi alloy by slow positron beam, J. Nucl. Mater. 458 (2015) 240-244
[18] X.B. Liu，R.S. Wang，J. Jiang，Y.C. Wu，C.H. Zhang，A. Ren，C.L. Xu, and W.J. Qian, Slow positron beam and nanoindentation study of irradiation-related defects in reactor vessel steels, J. Nucl. Mater. 451 (2014) 249-254
[19] J. Baram, and M. Rosen, Annihilation of positrons in FCC cold-worked polycrystals, phys. stat. sol. (a). 16 (1973) 263-272
[20] M. ABDELRAHMAN, Estimation of dislocation concentration in plastically deformed Al-Li based alloy by positron annihilation, Jpn. J. Appl. Phys 1. 36 (1997) 6530-3532
[21] K. Morishita，R. Sugano, and B.D. Wirth, MD and KMC modeling of the growth and shrinkage mechanisms of helium-vacancy clusters in Fe, J. Nucl. Mater. 323 (2003) 243-250
[22] K. Sato，T. Yoshiie，T. Ishizaki, and Q. Xu, Behavior of vacancies near edge dislocations in Ni and alpha-Fe: Positron annihilation experiments and rate theory calculations, Phys. Rev. B. 75 (2007) 11
[23]T. Troev，E. Popov，P. Staikov, and N. Nankov. Positron lifetime studies of defects in alpha-Fe containing helium. Physica Status Solidi C - Current Topics in Solid State Physics, Vol 6, No 11. Physica Status Solidi C-Current Topics in Solid State Physics. 62009. p. 2373-2375.
[24] D. Xu, and B.D. Wirth, Post-implantation thermal desorption of helium from poly- and single-crystalline iron, J. Nucl. Mater. 386-388 (2009) 395-399
[25] D.H. Xu，T. Bus，S.C. Glade, and B.D. Wirth, Thermal helium desorption spectrometry of helium-implanted iron, J. Nucl. Mater. 367 (2007) 483-488
[26] K. Morishita，R. Sugano，B.D. Wirth, and T. Diaz de la Rubia, Thermal stability of helium–vacancy clusters in iron, Nuclear Instruments and Methods in Physics Research Section B: Beam Interactions with Materials and Atoms. 202 (2003) 76-81

[27] T. Ishizaki， Q. Xu， T. Yoshiie, and S. Nagata, The recovery of gas-vacancy-complexes in Fe irradiated with high energy H or He ions, Materials Transactions. 45 (2004) 9-12
[28] Y.X. Wang，Q. Xu，T. Yoshiie, and Z.Y. Pan, Effects of edge dislocations on interstitial helium and helium cluster behavior in α-Fe, J. Nucl. Mater. 376 (2008) 133-138